Histone H4 tail mediates allosteric regulation of nucleosome remodelling by linker DNA

Published in final edited form as:
Nature. 2014 August 14; 512(7513): 213–217. doi:10.1038/nature13380.

Histone H4 tail mediates allosteric regulation of nucleosome remodelling by linker DNA

William L. Hwang[1,2,3,6], **Sebastian Deindl**[1,4,6], **Bryan T. Harada**[1,2], and **Xiaowei Zhuang**[1,4,5]

[1]Howard Hughes Medical Institute, Harvard University, Cambridge, MA 02138, USA

[2]Graduate Program in Biophysics, Harvard University, Cambridge, MA 02138, USA

[3]Harvard/MIT MD-PhD Program, Harvard Medical School, Boston, MA 02115, USA

[4]Department of Chemistry and Chemical Biology, Harvard University, Cambridge, MA 02138, USA

[5]Department of Physics, Harvard University, Cambridge, MA 02138, USA

Abstract

ISWI-family remodelling enzymes regulate access to genomic DNA by mobilizing nucleosomes[1]. These ATP-dependent chromatin remodellers promote heterochromatin formation and transcriptional silencing[1] by generating regularly-spaced nucleosome arrays[2-5]. The nucleosome-spacing activity arises from regulation of nucleosome translocation by the length of extranucleosomal linker DNA[6-10], but the underlying mechanism remains unclear. Here, we studied nucleosome remodelling by human ACF, an ISWI enzyme comprised of a catalytic subunit, Snf2h, and an accessory subunit, Acf1[2,11-13]. We found that ACF senses linker DNA length through an interplay between its accessory and catalytic subunits mediated by the histone H4 tail of the nucleosome. Mutation of AutoN, an auto-inhibitory domain within Snf2h that bears sequence homology to the H4 tail[14], abolished the linker-length sensitivity in remodelling. Addition of exogenous H4-tail peptide or deletion of the nucleosomal H4 tail also diminished the linker-length sensitivity. Moreover, the accessory subunit Acf1 bound the H4-tail peptide and DNA in a manner that depended on its N-terminal domain, and lengthening the linker DNA in the nucleosome reduced the proximity between Acf1 and the H4 tail. Deletion of the N-terminal portion of Acf1 (or its homologue in yeast) abolished linker-length sensitivity in nucleosome remodeling and led to severe growth defects *in vivo*. Taken together, our results suggest a mechanism for nucleosome spacing where linker DNA sensing by Acf1 is allosterically transmitted to Snf2h through the H4 tail of the nucleosome. For nucleosomes with short linker DNA, Acf1 preferentially binds to the H4 tail, allowing AutoN to inhibit the ATPase activity of

Correspondence should be addressed to X.Z. zhuang@chemistry.harvard.edu.
[6]These authors contributed equally to this work

Supplementary Information is linked to the online version of the paper.

Author Contributions: W.L.H., S.D. and X.Z. designed the experiments, with input from B.T.H. W.L.H. and S.D. performed the experiments and data analysis. B.T.H. helped prepare the histones and nucleosomes. S.D., W.L.H., and X.Z. wrote the paper. X.Z. oversaw the project.

Author Information: The authors declare no competing financial interests.

Snf2h. As the linker DNA lengthens, Acf1 shifts its binding preference to the linker DNA, freeing the H4 tail to compete AutoN off the ATPase and thereby activating ACF.

The packaging of DNA into nucleosomes presents a substantial energy barrier that restricts access to the genomic DNA[15]. ISWI-family remodellers use the energy from ATP hydrolysis to disrupt histone-DNA contacts and reposition nucleosomes[1]. The catalytic subunits of ISWI enzymes possess an SF2-like ATPase that translocates DNA across the nucleosome[1]. The nucleosome translocation activity is further regulated by the accessory subunits of ISWI complexes[6,10,16]. Many ISWI remodellers exhibit a nucleosome spacing activity[2-5]. Critical to this spacing activity are two features of the nucleosome that modulate the activity of ISWI remodellers: (1) the N-terminal tail of histone H4[8,17-20], and (2) the length of the extranucleosomal linker DNA[6-10]. The unmodified H4 tail stimulates ISWI activity by relieving the auto inhibitory effect of the AutoN domain within the catalytic subunit[14]. H4 tail acetylation associated with transcriptionally active chromatin is thought to help prevent ISWI-induced nucleosome spacing at actively transcribed genes[17-19]. Regulation by the extranucleosomal linker DNA is responsible for generating the regularly-spaced nucleosome arrays important for heterochromatin formation. Shortening the linker DNA reduces the remodelling activity of nucleosome-spacing ISWI enzymes[6-10]. As a result, nucleosomes are preferentially moved towards longer linkers to promote uniform spacing on nucleosome arrays. Interestingly, the catalytic activity of many ISWI-family enzymes is sensitive to linker DNA length sup to ∼60-70 bp[6-10], consistent with the inter-nucleosome spacing of heterochromatin observed in human cells[21]. This linker-length sensing range substantially exceeds the binding footprint (20-30 bp) of the catalytic subunit[22,23], whereas the accessory subunits of ISWI complexes can bind linker DNA as far as ∼60 bp from the nucleosome edge[22]. However, it is unknown how accessory subunits communicate linker length information to the catalytic subunit to regulate remodelling activity. In this work, we investigate the mechanism underlying DNA linker-length sensing by a prototypical ISWI-family enzyme, human ACF.

To examine how linker DNA regulates nucleosome translocation by ACF, we reconstituted mononucleosomes with varying linker lengths (*n* = 20-78 bp) on the entry side but a constant exit-side linker length of 3 bp (Fig. 1a). We also constructed mononucleosomes with wildtype (wt) histone H4 and two H4 mutants: (1) H4 tail deletion (H4Δ1-19), and (2) H4 with K16A mutation (H4K16A). We refer to nucleosome constructs with the following nomenclature: [wt H4/H4Δ1-19/H4K16A, *n* bp] for nucleosomes with *n* bp of DNA on the entry side and an octamer containing wt H4, H4Δ1-19, or H4K16A. We detected ACF-catalysed nucleosome translocation using fluorescence resonance energy transfer (FRET) by labelling the end of the exit-side linker DNA with the FRET acceptor Cy5, and the histone H2A with the FRET donor Cy3 (Fig. 1a)[24].

We first compared the remodelling kinetics of [wt H4, 78 bp], [wt H4, 40 bp], [wt H4, 20 bp], and [H4Δ1-19, 78 bp] nucleosomes using an ensemble FRET assay[6]. Upon addition of ACF and ATP, the FRET efficiency decreased as DNA was translocated towards the exit side (Fig. 1b and Extended Data Fig. 1a). As expected, the remodelling rate decreased as the

linker DNA was shortened and deletion of the H4 tail drastically reduced the remodelling activity (Fig. 1b).

To identify which step (s) of the remodelling process are regulated, we monitored the remodelling of individual nucleosomes using single-molecule FRET[24,25]. Single-nucleosome remodeling traces featured incremental translocation of DNA to the exit side interrupted by kinetic pauses (Fig. 1c and Extended Data Fig. 2a,b). The first pause occurred after ∼7 bp of DNA translocation and the second pause occurred after an additional ∼3 bp of translocation, consistent with previous findings[24,26]. Moreover, the step sizes did not change with linker DNA length or histone H4 modification (Extended Data Fig. 2a,b). We divided the remodelling time trace into two translocation phases (T1, T2), during which the FRET efficiency decreased, and two pause phases (P1, P2) without appreciable FRET change (Fig. 1c). Notably, the DNA translocation rates between pauses did not change, whereas the pause-phase exit rates decreased dramatically when the linker DNA was shortened (Fig. 1d and Extended Data Fig. 2c). Moreover, the dependence of remodelling kinetics on entry-side linker lengths of mononucleosomes was quantitatively similar to the dependence on inter-nucleosome linker lengths of dinucleosomes (Extended Data Fig. 3), validating the use of mononucleosomes as a model system to study linker-length sensitivity. Interestingly, the H4 tail appeared to regulate the same phase of the remodelling process as the linker DNA (Fig. 1e). The H4K16A mutation and H4 tail deletion (H4Δ1-19) decreased the pause-phase exit rate by ∼2 and ∼20 fold, respectively (Fig. 1e). In contrast, neither modification had any appreciable effect on the translocation rates between pauses (Fig. 1e).

The above results indicate that both linker DNA and the H4 tail regulate the remodelling rate by changing the duration of pause phases, suggesting that these nucleosome features may impinge on an inhibitory mechanism that prevents the initiation of the DNA translocation phases. It has been shown that although the ISWI ATPase domain can translocate nucleosomes autonomously[27], the catalytic subunit contains two well-conserved autoregulatory domains, AutoN and NegC, which inhibit ATP hydrolysis and its coupling to DNA translocation, respectively[14]. The AutoN inhibition can be relieved by the H4 tail whereas the NegC inhibition can be relieved by binding of the HAND-SANT-SLIDE module to linker DNA[14]. Could the regulation of remodelling by linker DNA length occur through these inhibitory domains?

To address this question, we first examined the role of the NegC domain. Surprisingly, deletion of the NegC domain in the ACF complex (ΔNegC ACF) did not substantially affect the dependence of remodelling kinetics on linker DNA lengths ranging from 20 to 78 bp (Fig. 2a, b and Extended Data Fig. 4a). Removing the H4 tail dramatically reduced the remodelling rates of both wt and ΔNegC ACF (Fig. 2b). These results suggest that the NegC domain does not play a substantial role in linker length sensing by the ACF complex. In contrast, the isolated Snf2h catalytic subunit exhibited a short-range (20-40 bp) linker length sensitivity that depended on NegC (Extended Data Fig. 5), in a manner similar to the *Drosophila* ISWI, which lacks any accessory subunit[14].

Next, we mutated the AutoN domain with two point substitutions (R142A and R144A) in the ACF complex (AutoN-2RA ACF; Fig. 3a and Extended Data Fig. 4a). AutoN bears

sequence homology to the H4 tail, which can compete the inhibitory AutoN domain off the ATPase, and the 2RA mutation in AutoN is expected to diminish the H4 tail dependence of remodelling by ISWI enzymes[14]. Remarkably, this mutation not only increased the remodelling rate of nucleosomes lacking the H4 tail, but also completely abolished the linker-length dependence of remodelling by specifically increasing the remodelling rate of short-linker nucleosomes (Fig. 3b,c and Extended Data Fig. 6). These results suggest an essential role for AutoN in linker length sensing by the ACF complex.

Since AutoN competes with the H4 tail for binding to the ATPase[14], we considered the possibility that this competition is involved in sensing linker DNA length and hypothesized that the H4 tail is only available to compete AutoN off the ATPase when the linker DNA is sufficiently long. Consistent with this hypothesis, adding exogenous H4-tail peptide, which should help compete AutoN off the ATPase when the nucleosomal H4 tail is unavailable, specifically increased the remodelling rate of short-linker nucleosome ([wt H4, 40 bp]) by wt ACF (Fig. 3d). Furthermore, deletion of the nucleosomal H4 tail, in addition to slowing down remodelling, abolished the dependence of remodelling rate on linker DNA length (Fig. 3e). These results indicate that the H4 tail is indeed involved in linker DNA sensing.

Because the catalytic subunits of ISWI-family enzymes only interact with ~20-30 bp of extranucleosomal DNA, the linker-length sensitivity of ACF cannot be accounted for by the catalytic subunit alone. Our findings raise the intriguing possibility of a linker-length sensing mechanism where the accessory subunit Acf1 interacts with the H4 tail in a linker-length dependent manner, which modulates the H4 tail availability for competing with AutoN. To test this possibility, we generated two Acf1 mutants, ΔC-term Acf1 and ΔN-term Acf1, in which 134 residues at the C-terminus or 371 residues at the N-terminus were deleted, respectively (Extended Data Fig. 7a and Fig. 4a). Because the central region of Acf1 required for Snf2h binding[16,28] was not deleted, both mutants were able to form complexes with Snf2h, which are referred to as ΔC-term and ΔN-term ACF (Extended Data Fig. 4b).

We first probed which region of Acf1 interacts with the H4 tail by comparing the binding affinities of wt, ΔC-term and ΔN-term Acf1 for the H4-tail peptide using a fluorescence anisotropy assay. Interestingly, wt Acf1 exhibited specific, nanomolar affinity for the H4-tail peptide (Fig. 4b and Extended Data Fig. 7b) that was not substantially altered upon deletion of the C-terminal region (Extended Data Fig. 7c), but was completely lost upon deletion of the N-terminal portion (Fig. 4b). These results indicate that Acf1 interacts with the H4 tail likely through its N-terminal region. Acf1 also bound double-stranded DNA and deletion of the N-terminal region abolished this interaction too (Extended Data Fig. 8), consistent with the previous finding that the WAC motif within the N-terminal region is important for binding of ACF to the linker DNA[28]. Given the distinct properties of DNA and the H4 tail, their specific binding interfaces within Acf1 N-term are likely distinct.

Next, we investigated nucleosome remodelling by the ΔC-term and ΔN-term ACF complexes. Notably, the ΔC-term mutation did not substantially alter the dependence of remodelling kinetics on linker DNA length (Extended Data Fig. 7d), whereas the linker-length sensitivity was eliminated in the ΔN-term ACF complex (Fig. 4c,d). This finding is

consistent with the specific affinity of Acf1 N-term for the H4 tail (Fig. 4b). Furthermore, if the loss of linker-length sensitivity was simply a result of losing the linker DNA binding affinity of Acf1, ΔN-term ACF should demonstrate inefficient remodelling for all linker DNA lengths. Instead, ΔN-term ACF remodelled both short- and long-linker nucleosomes at rates close to the rate with which wt ACF remodelled long-linker nucleosomes (Fig. 4c,d), suggesting that deletion of Acf1 N-term disabled a mechanism that inhibits remodelling at short linker lengths. ΔN-term ACF also maintained the H4-tail requirement in remodelling (Fig. 4c).

Since Acf1 has affinity to both DNA and the H4 tail, a plausible interpretation of the above observations is that nucleosomal linker DNA and H4 tail are in competition for binding to the N-terminal region of Acf1 and that this competition is modulated by the length of the linker DNA. Only when the linker is sufficiently short does Acf1 preferentially bind to the H4 tail, making it unavailable to compete with the inhibitory AutoN. Deletion of Acf1 N-term diminishes the Acf1-H4 tail interaction such that the H4 tail is equally available to activate the ATPase at both short and long linker DNA lengths. We therefore probed the linker-length dependence of the proximity between Acf1 and the H4 tail in ACF-bound nucleosomes featuring a cysteine-reactive crosslinker on the H4 tail. Specific H4-Acf1 crosslinking product was clearly observed as a band with reduced electrophoretic mobility compared to non-crosslinked Acf1 (Fig. 4e and Extended Data Fig. 9). Remarkably, the Acf1-H4 crosslinking efficiency decreased substantially with increasing linker DNA length (Fig. 4e), supporting our model that the Acf1-H4 tail interaction is modulated by the linker DNA length. In contrast, the H4-Snf2h crosslinking efficiency did not change substantially with linker DNA length, likely because Snf2h remains sufficiently close to the H4 tail regardless of the linker DNA length, which allows crosslinking even when the H4 tail was not specifically bound to its binding pocket on Snf2h.

Finally, we tested the physiological importance of the N-terminal region of Acf1 by studying the role of its homologue in yeast[29]. Yeast ISW2 is functionally similar to ACF. It is composed of a catalytic subunit (Isw2) that is homologous to Snf2h and three accessory subunits (Itc1, Dpb4 and Dls1), among which Itc1 is homologous to Acf1. We generated three mutant yeast strains: (1) deletion of the entire *itc1* gene (Δ*itc1*), (2) deletion of only the portion of *itc1* that encodes the N-terminal region of Itc1 equivalent to Acf1 N-term (Δ*itc1-Nterm*), and (3) a rescue strain that was derived from the Δ*itc1-Nterm* strain by deleting the remainder of *itc1* (rescue-Δ*itc1*). Both Δ*itc1* and rescue-Δ*itc1* showed growth rates similar to that of the wt strain (Fig. 4f), consistent with previous observations[29]. In contrast, the Δ*itc1-Nterm* strain displayed dramatically slower growth (Fig. 4f), consistent with an aberrant chromatin-misregulation phenotype.

Taken together, our results suggest a nucleosome-spacing mechanism for ACF in which the linker DNA length is sensed by the Acf1 accessory subunit and allosterically transmitted to the Snf2h catalytic subunit through the H4 tail of the nucleosome (Fig. 4g). Surprisingly, Acf1 and the AutoN domain of Snf2h function collectively in DNA linker-length sensing. When the linker DNA is short, Acf1 preferentially binds to and sequesters the H4 tail, making it unavailable to compete its sequence homologue, AutoN, off the ATPase. Hence, the ATPase activity is inhibited by AutoN. As the linker DNA length increases, Acf1 shifts

its binding preference to the linker DNA and releases the H4 tail, allowing it to compete AutoN off the ATPase and activate ACF. This competition between the H4 tail and linker DNA for Acf1 binding likely involves the N-terminal region of Acf1. It is interesting to note that linker DNA sensing occurs during the pause phases when the ATPase domain is not actively translocating DNA, suggesting that AutoN engages the ATPase domain during the pauses. In order to exit the pauses, the H4 tail is required to relieve the inhibitory effect of AutoN. The re-engagement of AutoN with the ATPase domain after each translocation phase would give ACF an opportunity to periodically sense the linker DNA length. Such frequent sensing may allow a more efficient nucleosome spacing, as previously hypothesized[30]. The linker DNA and the H4 tail are two important substrate features that regulate nucleosome remodelling by ISWI-family enzymes, the former enabling uniform nucleosome spacing for heterochromatin formation and the latter specifying regions of chromatin for silencing. Our results now reveal an unexpected convergence of the regulatory pathways defined by these two distinct nucleosome features.

Methods Summary

Detailed descriptions of nucleosome and ACF preparation, as well as single-molecule and ensemble FRET, fluorescence anisotropy, protein crosslinking, and yeast experiments are described in the Online Methods. Briefly, various nucleosome constructs were reconstituted using Cy3-labelled histone octamers and Cy5-labelled DNA with a biotin moiety for surface anchoring. DNA was generated by PCR or by annealing and ligating a set of overlapping, complementary oligonucleotides (Extended Data Fig. 10). Histone octamer, nucleosomes, Acf1, Snf2h and ACF complexes were reconstituted and purified as described previously[6,7,24]. Mutant yeast strains were generated in the BY4741 background. Single-molecule FRET measurements were performed with a custom-built microscope setup. Ensemble FRET was performed using a Cary Eclipse Fluorescence Spectrophotometer. Fluorescence anisotropy measurements were carried out using a SpectraMax microplate reader. Crosslinking experiments were carried out using nucleosomes with a cysteine-reactive crosslinker BM $(PEG)_3$ at the H4 tail N-terminus and reaction products were analyzed by SDS-PAGE.

Extended Data Figures

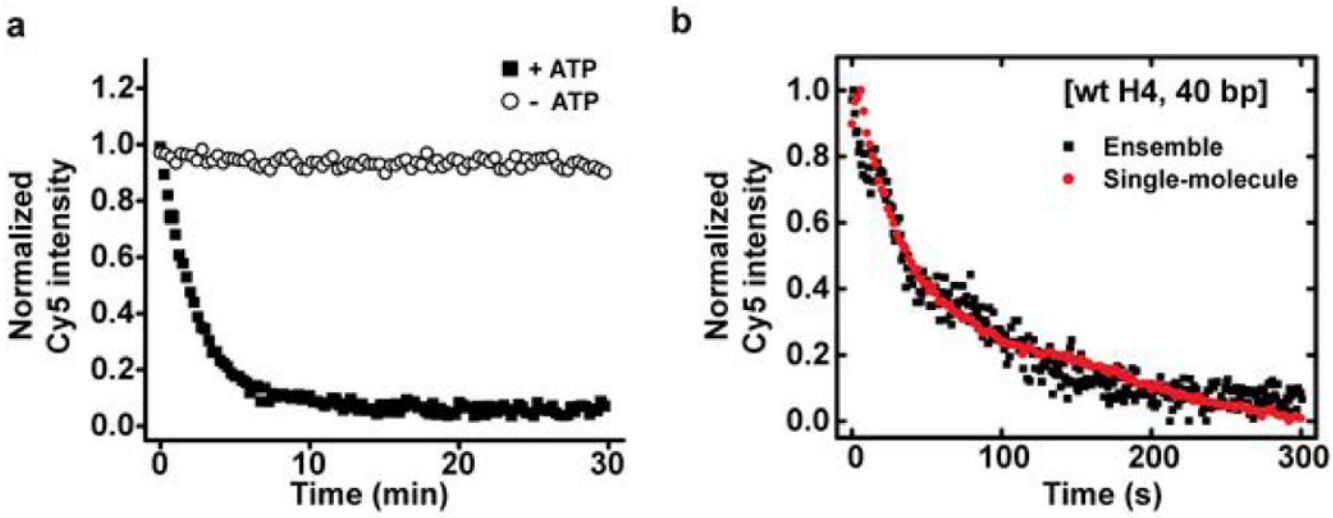

Extended Data Figure 1. Control experiments to test the effect of ATP and surface-anchoring on nucleosome remodelling

a, Ensemble remodelling time courses of [wt H4, 78 bp] nucleosomes by 10 nM ACF with 5 μM ATP (filled symbols) or without (open symbols) ATP. Nucleosome translocation is monitored by the emission intensity of the FRET acceptor Cy5 under constant 532 nm illumination that excites the FRET donor Cy3. **b**, Comparison of the average remodelling kinetics for surface-anchored [wt H4, 40 bp] nucleosomes (measured by the single-molecule assay, > 250 nucleosomes) and freely diffusing [wt H4, 40 bp] nucleosomes in solution (measured by the ensemble assay). [ACF] = 5 nM and [ATP] = 20 μM.

601 sequence
Top Strand (5′ to 3′)
CTGGAGAATCCCGGTCTGCAGGCCGCTCAATTGGTCGTAGACAGCTCTAGCACCGCTTAAACGCACGTACGCGCTGTCCCCCGCGTTTTA
ACCGCCAAGGGGATTACTCCCTAGTCTCCAGGCACGTGTCAGATATATACATCCTGT
Bottom Strand (5′ to 3′)
ACAGGATGTATATATCTGACACGTGCCTGGAGACTAGGGAGTAATCCCCTTGGCGGTTAAAACGCGGGGGACAGCGCGTACGTGCGT
TTAAGCGGTGCTAGAGCTGTCTACGACCAATTGAGCGGCCTGCAGACCGGGATTCTCCAG

Mononucleosome with 20 bp linker DNA
Top Strand (5′ to 3′) Cy5-GCC-601-GCATGTATTGAACAGCGACC
Bottom Strand (5′ to 3′) Biotin-CCCGCCCGCCAAAAAAAAAAAAAAAAAAAAAAAAAAAAAAGGTCGCTGTTCAATACATGC-601-GGC

Mononucleosome with 40 bp linker DNA
Top Strand (5′ to 3′) Cy5-GCC-601-GCATGTATTGAACAGCGACCTTGCCGGTGCCAGTCGGATA
Bottom Strand (5′ to 3′) Biotin-
CCCGCCCGCCAAAAAAAAAAAAAAAAAAAAAAAAAAAAAATATCCGACTGGCACCGGCAAGGTCGCTGTTCAATACATGC-601-GGC

Mononucleosome with 45 bp linker DNA
Top Strand (5′ to 3′) Cy5-GCC-601-GCATGTATTGAACAGCGACCTTGCCGGTGCCAGTCGGATAGTGTT
Bottom Strand (5′ to 3′) Biotin-
CCCGCCCGCCAAAAAAAAAAAAAAAAAAAAAAAAAAAAAAACACTATCCGACTGGCACCGGCAAGGTCGCTGTTCAATACA TGC-601-GGC

Mononucleosome with 50 bp linker DNA
Top Strand (5′ to 3′) Cy5-GCC-601-GCATGTATTGAACAGCGACCTTGCCGGTGCCAGTCGGATAGTGTTCCGAG
Bottom Strand (5′ to 3′) Biotin-
CCCGCCCGCCAAAAAAAAAAAAAAAAAAAAAAAAAAAAAAACTCGGAACACTATCCGACTGGCACCGGCAAGGTCGCTGTTCA ATACATGC-601-GGC

Mononucleosome with 60 bp linker DNA
Top Strand (5′ to 3′) Cy5-GCC-601-GCATGTATTGAACAGCGACCTTGCCGGTGCCAGTCGGATAGTGTTCCGAGCTCCCACTCT
Bottom Strand (5′ to 3′)Biotin-
CCCGCCCGCCAAAAAAAAAAAAAAAAAAAAAAAAAAAAAAAGAGTGGGAGCTCGGAACACTATCCGACTGGCACCGGCAAGGT
CGCTGTTCAATACATGC-601-GGC

Mononucleosome with 78 bp linker DNA
Top Strand (5′ to 3′) Cy5-GCC-601-
GCATGTATTGAACAGCGACCTTGCCGGTGCCAGTCGGATAGTGTTCCGAGCTCCCACTCTAGAGGATCCCCGGGTACC
Bottom Strand (5′ to 3′)Biotin-
CCCGCCCGCCAAAAAAAAAAAAAAAAAAAAAAAAAAAAAAGGTACCCGGGGATCCTCTAGAGTGGGAGCTCGGAACACTAT
CCGACTGGCACCGGCAAGGTCGCTGT TCAATACATGC-601-GGC

Dinucleosome with 40 bp linker DNA
Top Strand (5′ to 3′) Cy5-GCC-601-GCTTGTATTGCCCAGCGACCTTGCCCGTGCCAGTCGGATA-601*-
GCATGTATTGAACAGCGACCTTGCCGGTGCCA GTCGGATA
Bottom Strand (5′ to 3′) Biotin-TATCCGACTGGCACCGGCAAGGTCGCTGTTCAATACATGC-601*-
TATCCGACTGGCACGGGCAAGGTCGCTGGGCAAT ACAAGC-601-GGC

Dinucleosome with 78 bp linker DNA
Top Strand (5′ to 3′) Cy5-GCC-601-
GCATGTATTGAACAGCGACCCTGCCCGTGCCAGACCGTTAGTGTTCCGACCTCCCACCCTAGAGGATCCCCGGGTACC -601*-
GCATGTATTGAACAGC GACCTTGCCGGTGCCAGTCGGATA
Bottom Strand (5′ to 3′) Biotin-TATCCGACTGGCACCGGCAAGGTCGCTGTTCAATACATGC-601*-
GGTACCCGGGGATCCTCTAGGGTGGGAGGTCGGA ACACTAACGGTCTGGCACGGGCAGGGTCGCTGTTCAATACATGC-601-GGC

Symmetric mononucleosome with 20 bp linker DNA
Top Strand (5′ to 3′) Cy5-GGACCCTATACGCGGCCGCC-601-GCATGTATTGAACAGCGACC
Bottom Strand (5′ to 3′) GGTCGCTGTTCAATACATGC-601-GGCGGCCGCGTATAGGGTCC

Symmetric mononucleosome with 40 bp linker DNA
Top Strand (5′ to 3′) Cy5-GAGTTCATCCCTTATGTGATGGACCCTATACGCGGCCGCC-601-
GCATGTATTGAACAGCGACCTTGCCGGTGCCAGTCGGATA
Bottom Strand (5′ to 3′) TATCCGACTGGCACCGGCAAGGTCGCTGTTCAATACATGC-601-
GGCGGCCGCGTATAGGGTCCATCACATAAGGGATGAACTC

Symmetric mononucleosome with 78 bp linker DNA
Top Strand (5′ to 3′) Cy5-
GGATCCTAATGACCAAGGAAAGCATGATTCTTCACACCGAGTTCATCCCTTATGTGATGGACCCTATACGCGGCCGCC-601-GCA
TGTATTGAACAGCGACCTTGCCGGTGCCAGTCGGATAGTGTTCCGAGCTCCCACTCTAGAGGATCCCCGGGTACC
Bottom Strand (5′ to 3′)
GGTACCCGGGGATCCTCTAGAGTGGGAGCTCGGAACACTATCCGACTGGCACCGGCAAGGTCGCTGTTCAATACATGC-601- GGC
GGCCGCGTATAGGGTCCATCACATA AGGGATGAACTCGGTGTGAAGAATCATGCTTTCCTTGGTCATTAGGATCC

Extended Data Figure 2. Translocation step sizes and dwell time distributions of translocation and pauses phases during nucleosome remodelling

a, Histogram of FRET levels for the initial position and pause positions of [wt H4, 40 bp] nucleosomes upon remodelling by ACF. The histogram was fit by multiple Gaussian peaks (black line) and the peak values were used to compute the average translocation distances between pauses. The translocation distances can be quantified using a calibration curve of FRET efficiency versus exit-side linker DNA length[24,26], yielding at 7.0 bp step size between the initial position and the first pause and a 3.4 bp step size between the first pause

and the second pause. **b**, Step sizes for various mononucleosomes and dinucleosomes. The dinucleosome constructs, [wt H4, 40 bp, wt H4] and [wt H4, 78 bp, wt H4], are each composed of one FRET-labelled nucleosome and one unlabelled nucleosome, spaced by 40 bp and 78 bp of internucleosomal linker DNA, respectively. The flanking linker DNA is 3 bp on the side of the FRET-labelled nucleosome and 40 bp on the side of the unlabelled nucleosome. The unlabelled nucleosome contains 2-nt ssDNA gaps at the SHL±2 sites to prevent translocation. Data are mean ± s.e.m derived from at least 100 remodelling traces from three independent experiments. **c**, Dwell time distributions for the first translocation phase, t_{T1}, and the first pause phase, t_{P1}, for nucleosomes with different lengths of linker DNA. [ACF] = 10 nM and [ATP] = 20 μM.

a

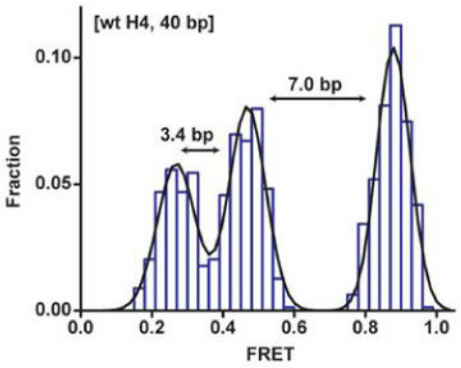

b

Nucleosome	1st Step (bp)	2nd Step (bp)
[wt H4, 40 bp]	7.0±0.1	3.4±0.2
[wt H4, 45 bp]	7.0±0.1	3.3±0.1
[wt H4, 50 bp]	7.1±0.1	3.4±0.1
[wt H4, 60 bp]	6.9±0.1	3.7±0.2
[wt H4, 78 bp]	7.2±0.1	3.5±0.1
[H4K16A, 78 bp]	7.0±0.1	3.3±0.1
[H4Δ1-19, 78 bp]	7.4±0.1	3.1±0.2
[wt H4, 40 bp, wt H4]	7.2±0.1	3.6±0.2
[wt H4, 78 bp, wt H4]	7.2±0.1	3.0±0.1

c

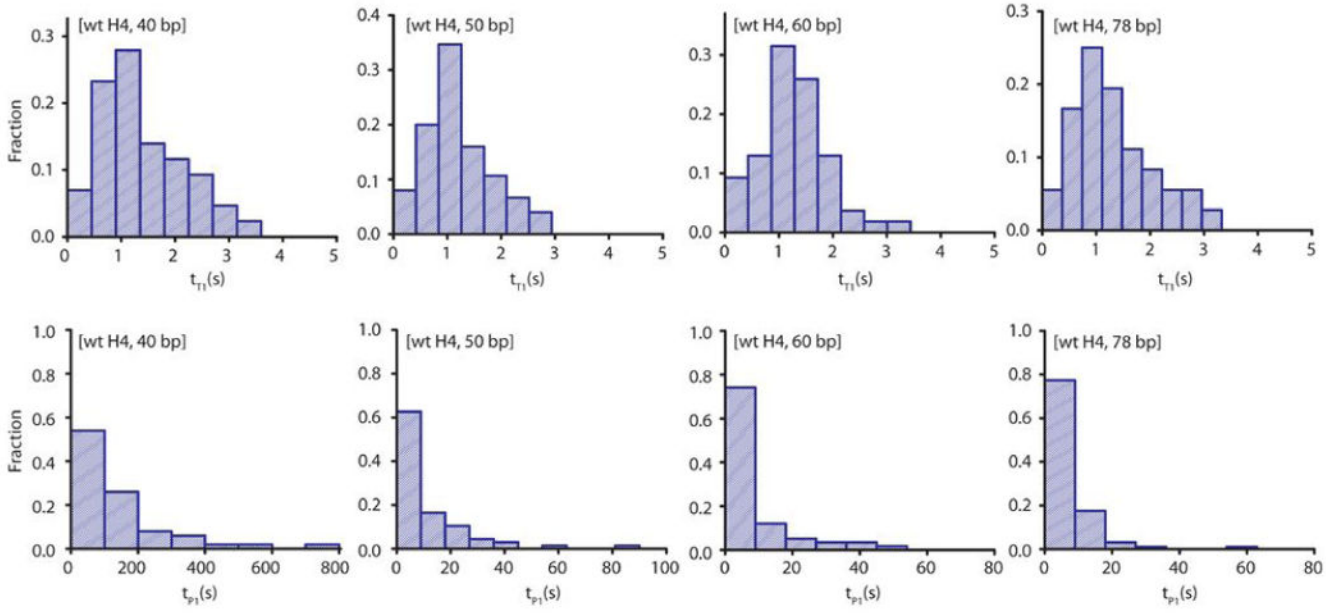

Extended Data Figure 3. DNA linker-length sensing by ACF is quantitatively similar for mononucleosomes and dinucleosomes

a, The dinucleosomes contain a distal FRET-labelled nucleosome and a proximal unlabelled nucleosome connected by *n* bp of internucleosomal linker DNA. The flanking linker DNA is

3 bp and 40 bp on the side of the FRET-labelled and the unlabelled nucleosome, respectively. To facilitate the study of translocation of the FRET-labelled nucleosome, we placed 2-nt ssDNA gaps at the SHL±2 sites of the proximal nucleosome to prevent its repositioning. **b**, Comparison of translocation and pause-phase exit rates for mononucleosomes (filled bars) and dinucleosomes (hashed bars) with 40 and 78 bp linker lengths. [ACF] = 10 nM and [ATP] = 20 μM. Data are mean ± s.e.m derived from at least 100 individual nucleosome remodelling traces from three independent experiments.

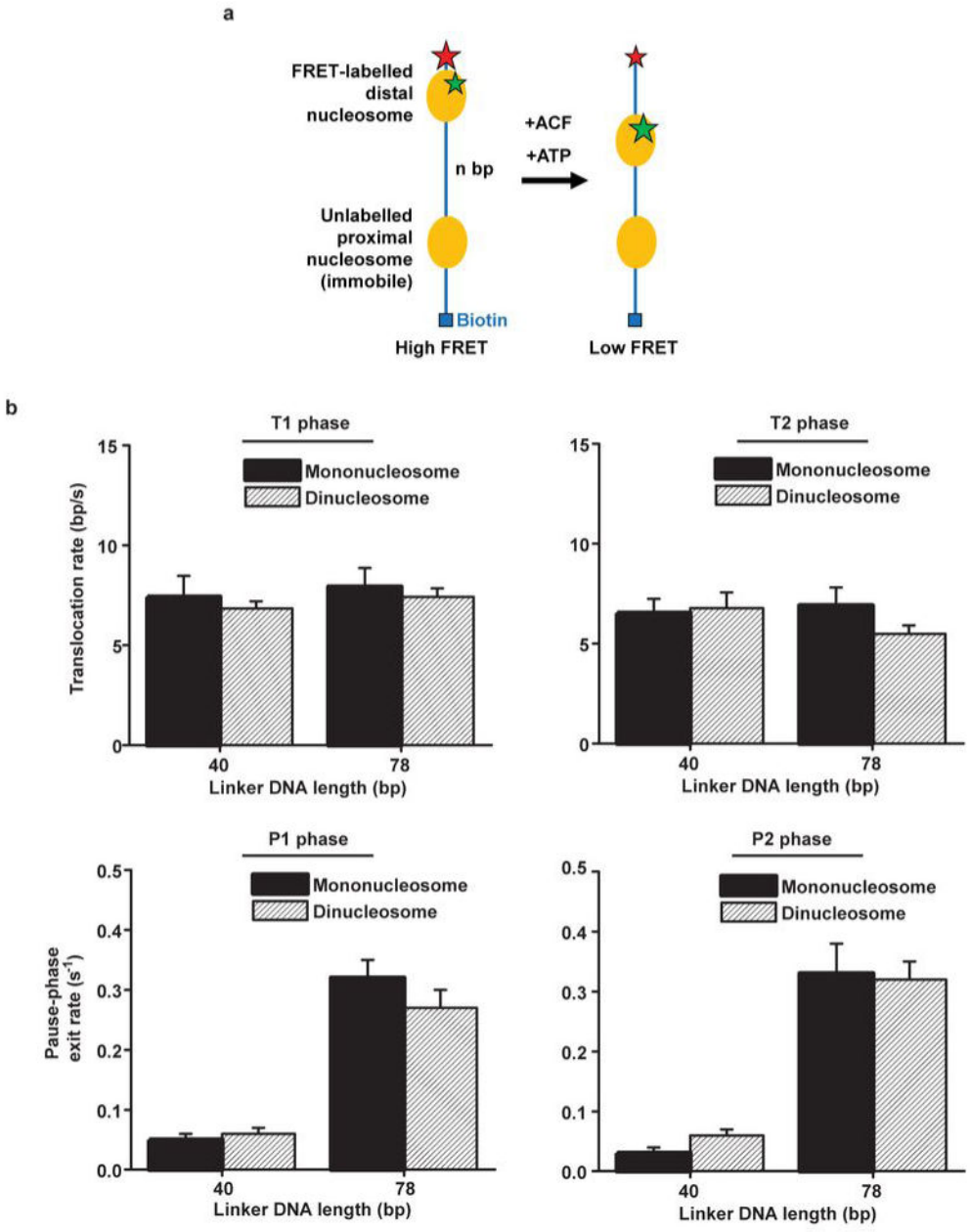

Extended Data Figure 4. SDS-PAGE analysis of wt, ΔNegC, AutoN-2RA, ΔN-term and ΔC-term ACF complexes

a, wt Snf2h, ΔNegC Snf2h, or AutoN-2RA Snf2h were co-expressed with Acf1-FLAG in Sf9 insect cells and purified by affinity chromatography. **b**, ΔN-term Acf1 or ΔC-term Acf1 was co-expressed with Snf2h-FLAG and purified by affinity chromatography. The presence of both Acf1 and Snf2h in each case indicated that wt SNF2h, ΔNegC SNF2h and AutoN-2RA SNF2h can all form complexes with Acf1 and that ΔN-term Acf1 and ΔC-term Acf1 can both form complexes with Snf2h.

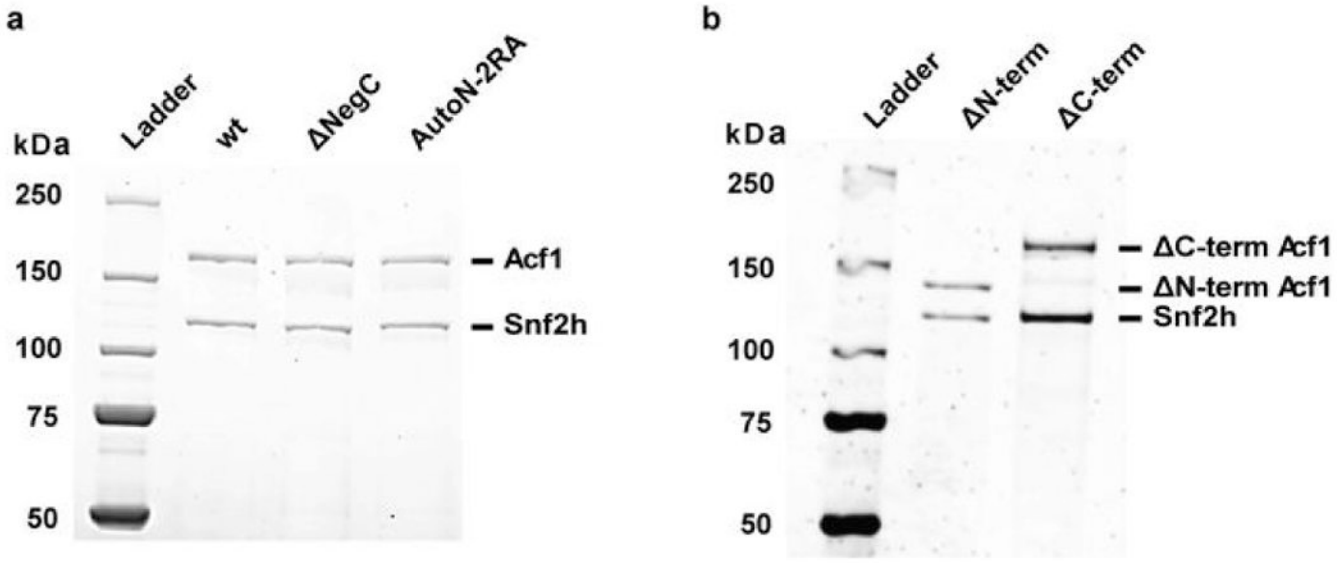

Extended Data Figure 5. Short-range linker-length sensing by the isolated Snf2h catalytic subunit requires the NegC domain

Ensemble remodelling time courses of [wt H4, 78 bp], [wt H4, 40 bp] and [wt H4, 20 bp] nucleosomes by 130 nM wt (**a**) or ΔNegC Snf2h (**b**) at 2 mM ATP.

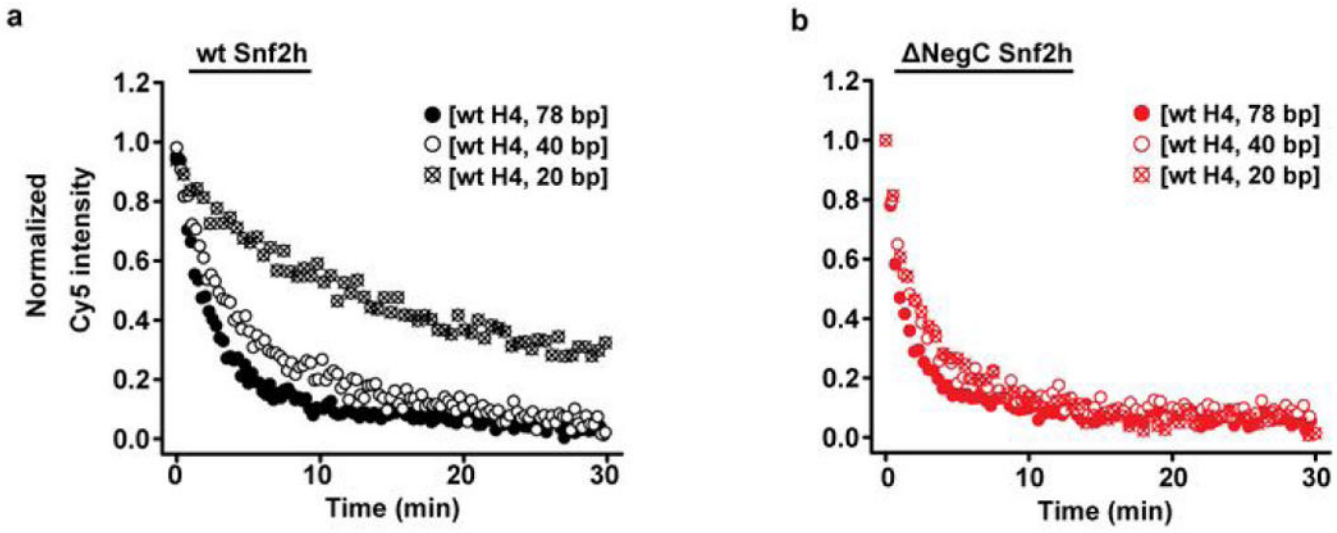

Extended Data Figure 6. Ensemble remodelling time courses of nucleosomes by wt and AutoN-2RA ACF at two different enzyme concentrations

a, Remodelling of [wt H4, 78 bp] and [wt H4, 40 bp] nucleosomes by 40 nM (top) and 10 nM (bottom) wt ACF. **b**, Remodelling of [wt H4, 78 bp] and [wt H4, 40 bp] nucleosomes by 40 nM (top) and 10 nM (bottom) AutoN-2RA ACF.

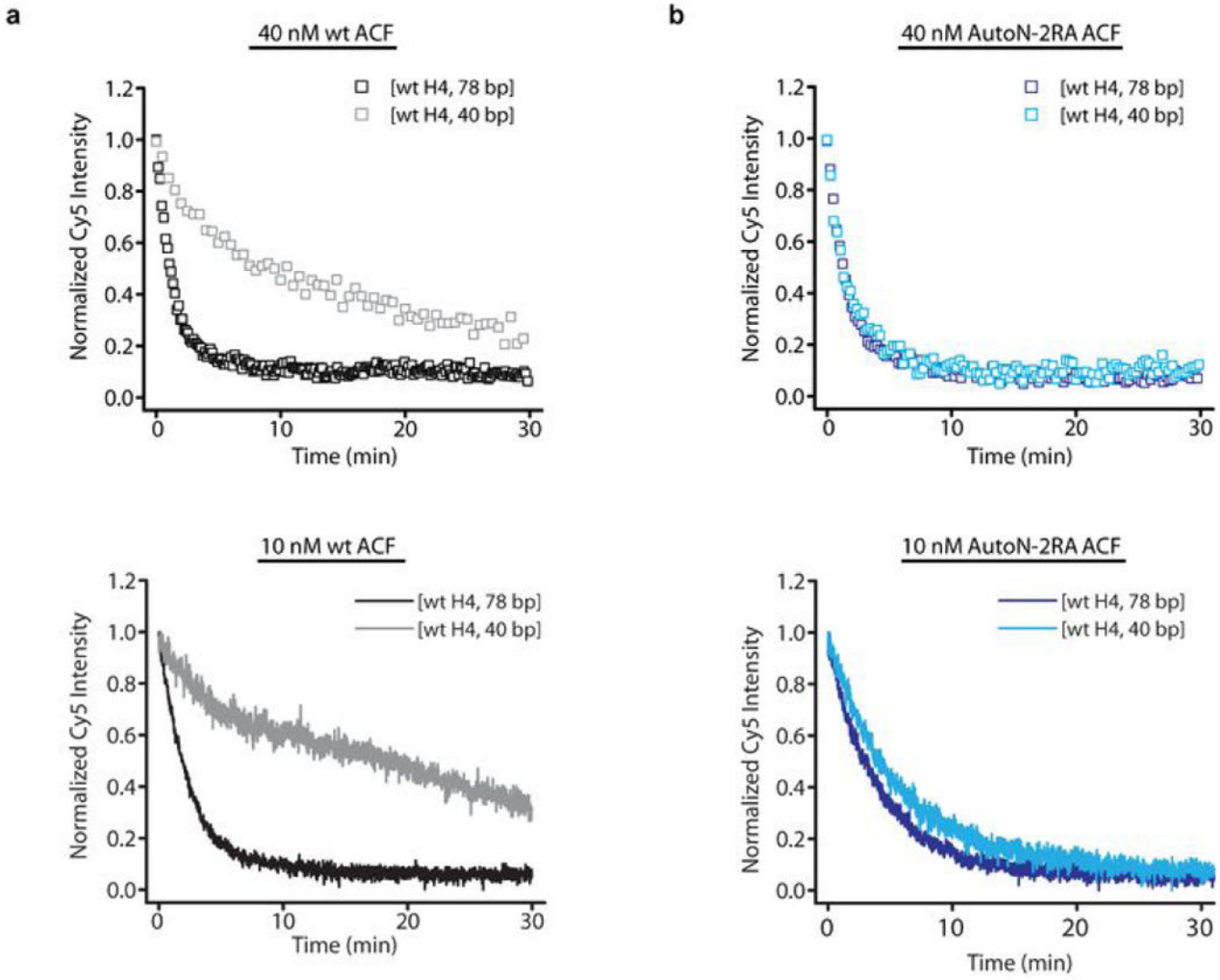

Extended Data Figure 7. The C-terminal region of Acf1 is not required for specific binding to the H4 tail or for linker-length sensing by the ACF complex

a, Domain maps of wt and ΔC-term Acf1 (residues 1423-1556 deleted). **b**, Fluorescence anisotropy of TMR-labelled wt or 2RA H4-tail peptide in the presence of varying amounts of wt Acf1. In the 2RA H4-tail peptide, two charged arginines in the basic patch of the H4-tail peptide corresponding to the 2RA mutation in AutoN were replaced with alanines. The K_d for the 2RA H4-tail peptide (41 ± 29 nM) is substantially higher than that of the wt H4-tail peptide (3 ± 9 nM). Data are presented as mean ± s.e.m. (errors report the 95% confidence interval, $n = 3$ three independent titration experiments). When excess unlabelled H4-tail peptide was added to compete the TMR-labelled peptide off Acf1, the fluorescence anisotropy was reduced to the background level in the absence of Acf1. **c**, Fluorescence

anisotropy of TMR-labelled H4-tail peptide in the presence of varying amounts of wt or ΔC-term Acf1. The measured K_d for ΔC-term Acf1 is 2 ± 7 nM, which is similar to that for wt Acf1 (3 ± 9 nM). Data are presented as mean ± s.e.m. (errors report the 95% confidence interval, *n* = 3 independent titration experiments). **d**, Ensemble remodelling time courses of [wt H4, 78 bp], [wt H4, 40 bp], and [H4Δ1-19, 78 bp] nucleosomes by 40 nM wt (balck/gray lines) and ΔC-term ACF (purple/light purple symbols) at 5 μM ATP.

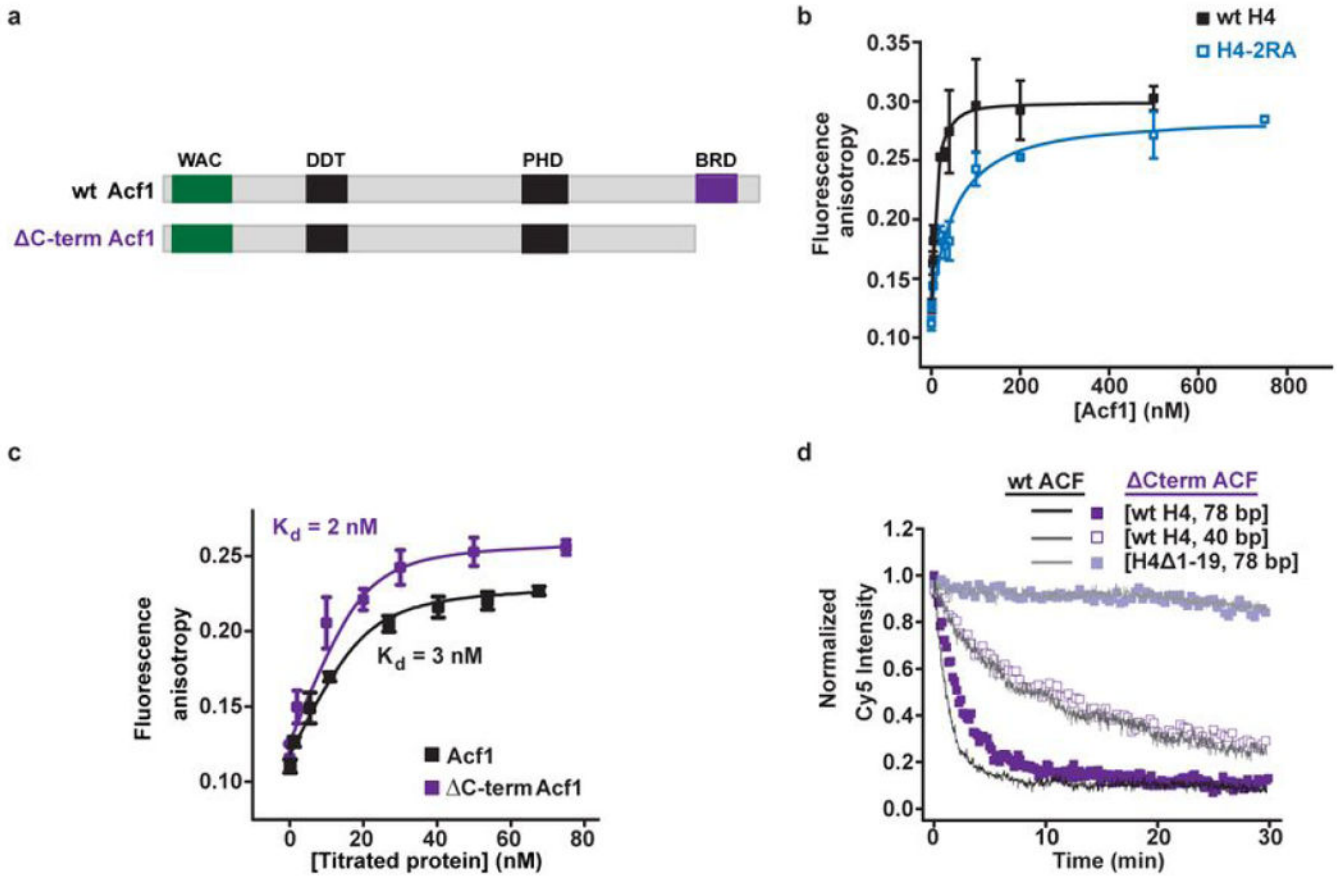

Extended Data Figure 8. Binding of dsDNA to Acf1 depends on its N-terminal region

Electrophoretic mobility of dsDNA (225 bp, 8 nM) in the presence or absence of 22 nM wt or ΔN-term Acf1. As a comparison, lanes 2 and 4 show Acf1 samples without the dsDNA.

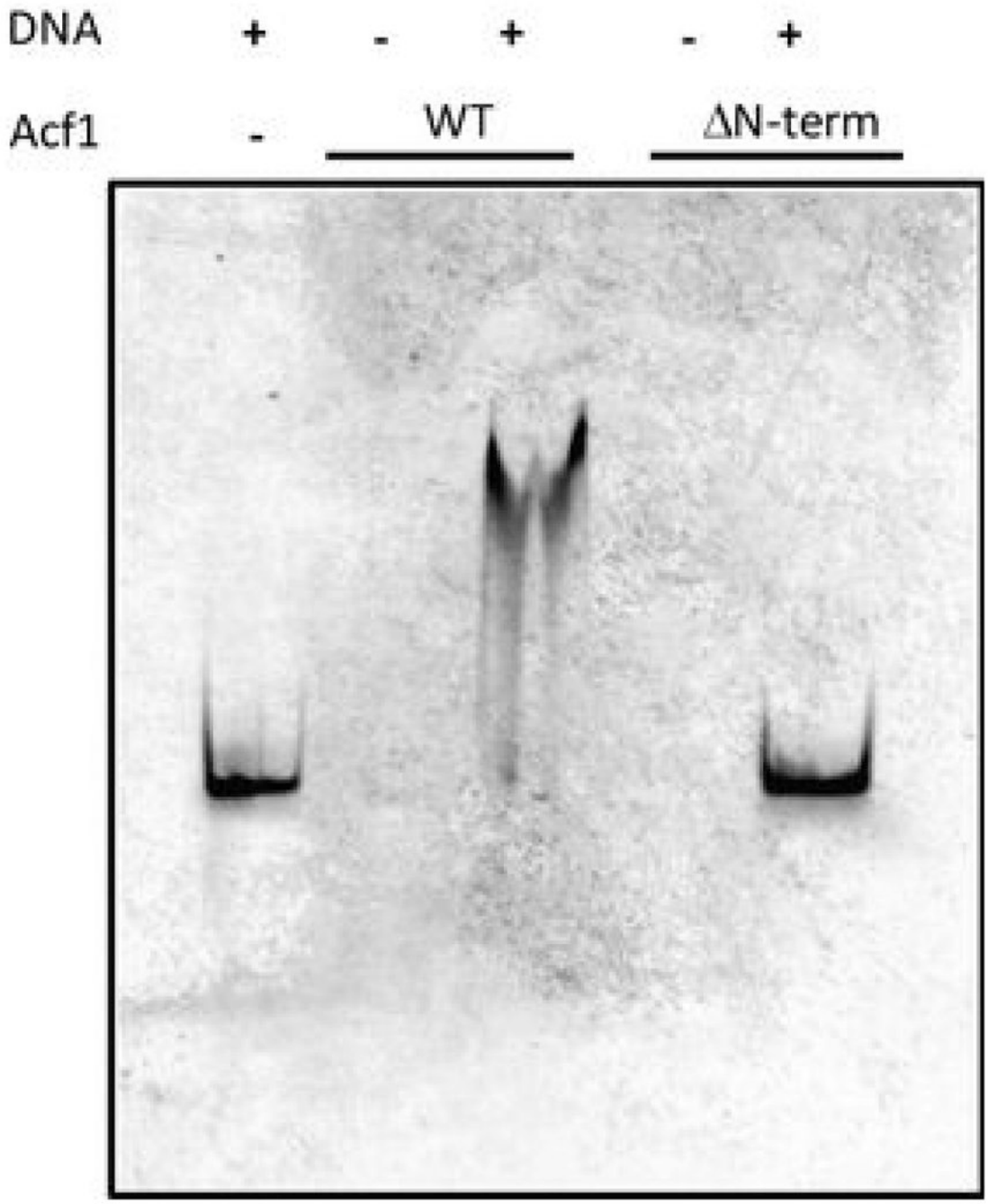

Extended Data Figure 9. α-histone H4 immunoblot analysis validates the formation of the Acf1-H4 crosslinked product

a, Left: SDS PAGE analysis of samples containing ACF alone or ACF with nucleosomes (20 bp linker DNA) that do not possess the cysteine-reactive crosslinker on the H4 tail. Both samples yield two distinct bands corresponding to the Acf1 and Snf2h subunits (180 kDa and 122 kDa, respectively). Additionally, histone bands at low molecular weights are present in the lane for the sample containing nucleosomes. Right: Corresponding immunoblot using α-H4 antibody. In the presence of nucleosomes without crosslinker, a

single H4 band is visible at ∼11 kDa corresponding to the histone itself. **b**, Top: Incubation of ACF and nucleosomes that contain a crosslinker at the H4 tail yield Acf1-H4 and Snf2h-H4 crosslinking bands. These bands are absent for ACF without addition of nucleosomes ("- nucleosomes") or upon addition of nucleosomes without a crosslinker. Proteolytic degradation of Acf1 gave rise to a fainter band immediately below Acf1. Bottom: α-histone H4 immunoblotting reveals specific Acf1-H4 and Snf2h-H4 bands that are absent for ACF without addition of nucleosomes ("- nucleosomes") or upon addition of nucleosomes without a crosslinker.

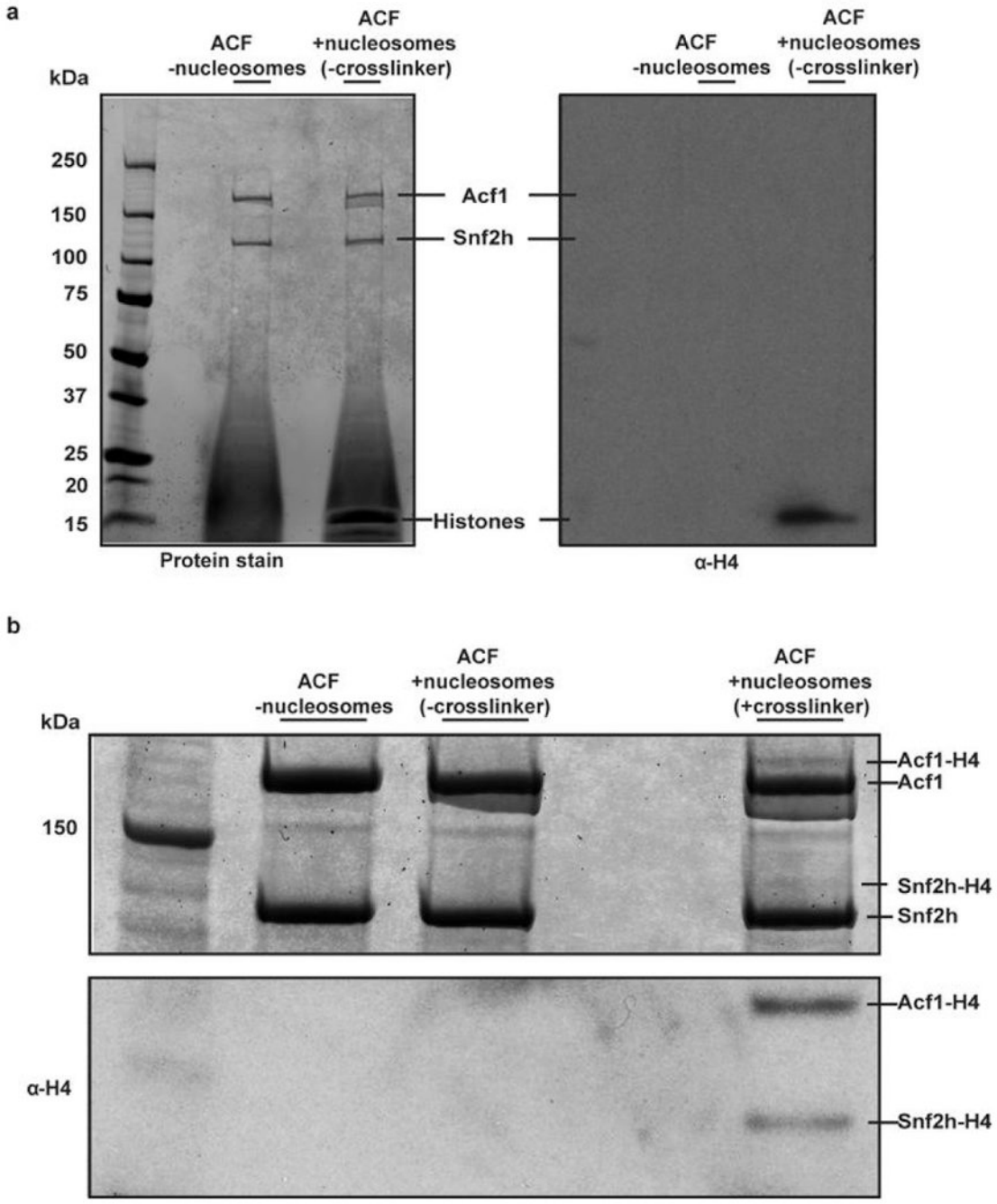

Extended Data Figure 10. DNA constructs for mononucleosomes and dinucleosomes

The 601 nucleosome positioning sequence is shown in green (601* represents the introduction of 2-nt gaps at nucleotides 53 and 54 in the top and bottom strands of the 601 positioning sequence, respectively). For mononucleosome DNA constructs, the ssDNA spacer used to circumvent surface effects in single-molecule FRET measurements is underlined. Constructs referred to as “mononucleosome or dinucleosome with *n* bp linker DNA” were used in single-molecule and bulk remodelling experiments. For ensemble remodelling experiments with mononucleosomes, the ssDNA spacer was omitted without

any appreciable change in the overall remodelling kinetics. Constructs referred to as "symmetric mononucleosomes with *n* bp linker DNA" were used in crosslinking experiments. Asymmetric constructs with the same linker length on one side of the nucleosome but only 3 bp of linker DNA on the other side displayed quantitatively similar crosslinking behaviour.

Acknowledgments

We thank G. Narlikar, T. Tsukiyama, J. Vaughan, J. Moffitt, and E. Sun for insightful discussions, S. Mukherji for assistance in designing the yeast experiments, K. L. Hwang, R. Magnusson, G. Hilinski, and J. McGee for assistance with protein biochemistry, and G. Narlikar for providing Snf2h and Acf1 expression vectors and purification protocols. This work was supported in part by the National Institutes of Health (GM105637 to X.Z.). W.L.H. acknowledges support from the NIH T32G007753 Training Grant. S.D. was a Merck Fellow of the Jane Coffin Childs Foundation. X.Z. is a Howard Hughes Medical Investigator.

References

1. Clapier CR, Cairns BR. The biology of chromatin remodeling complexes. Annu Rev Biochem. 2009; 78:273–304. [PubMed: 19355820]
2. Ito T, Bulger M, Pazin MJ, Kobayashi R, Kadonaga JT. ACF, an ISWI-containing and ATP-utilizing chromatin assembly and remodeling factor. Cell. 1997; 90:145–155. [PubMed: 9230310]
3. Varga-Weisz PD, Wilm M, Bonte E, Dumas K, Mann M, Becker PB. Chromatin-remodelling factor CHRAC contains the ATPases ISWI and topoisomerase II. Nature. 1997; 388:598–602. [PubMed: 9252192]
4. Tsukiyama T, Palmer J, Landel CC, Shiloach J, Wu C. Characterization of the Imitation Switch subfamily of ATP-dependent chromatin-remodeling factors in Saccharomyces cerevisiae. Genes & Development. 1999; 13:686–697. [PubMed: 10090725]
5. Langst G, Bonte EJ, Corona DF, Becker PB. Nucleosome movement by CHRAC and ISWI without disruption or trans-displacement of the histone octamer. Cell. 1999; 97:843–852. [PubMed: 10399913]
6. Yang JG, Madrid TS, Sevastopoulos E, Narlikar GJ. The chromatin-remodeling enzyme ACF is an ATP-dependent DNA length sensor that regulates nucleosome spacing. Nat Struct Mol Biol. 2006; 13:1078–1083. [PubMed: 17099699]
7. He X, Fan HY, Narlikar GJ, Kingston RE. Human ACF1 alters the remodeling strategy of SNF2h. J Biol Chem. 2006; 281:28636–28647. [PubMed: 16877760]
8. Dang W, Kagalwala MN, Bartholomew B. Regulation of ISW2 by concerted action of histone H4 tail and extranucleosomal DNA. Mol Cell Biol. 2006; 26:7388–7396. [PubMed: 17015471]
9. Stockdale C, Flaus A, Ferreira H, Owen-Hughes T. Analysis of nucleosome repositioning by yeast ISWI and Chd1 chromatin remodeling complexes. J Biol Chem. 2006; 281:16279–16288. [PubMed: 16606615]
10. He X, Fan HY, Garlick JD, Kingston RE. Diverse regulation of SNF2h chromatin remodeling by noncatalytic subunits. Biochemistry. 2008; 47:7025–7033. [PubMed: 18553938]
11. Ito T, Levenstein ME, Fyodorov DV, Kutach AK, Kobayashi R, Kadonaga JT. ACF consists of two subunits, Acf1 and ISWI, that function cooperatively in the ATP-dependent catalysis of chromatin assembly. Genes Dev. 1999; 13:1529–1539. [PubMed: 10385622]
12. LeRoy G, Loyola A, Lane WS, Reinberg D. Purification and characterization of a human factor that assembles and remodels chromatin. J Biol Chem. 2000; 275:14787–14790. [PubMed: 10747848]
13. Poot RA, et al. HuCHRAC, a human ISWI chromatin remodelling complex contains hACF1 and two novel histone-fold proteins. EMBO J. 2000; 19:3377–3387. [PubMed: 10880450]
14. Clapier CR, Cairns BR. Regulation of ISWI involves inhibitory modules antagonized by nucleosomal epitopes. Nature. 2012; 492:280–284. [PubMed: 23143334]

15. Killian JL, Li M, Sheinin MY, Wang MD. Recent advances in single molecule studies of nucleosomes. Curr Opin Struct Biol. 2012; 22:80–87. [PubMed: 22172540]
16. Eberharter A, Vetter I, Ferreira R, Becker PB. ACF1 improves the effectiveness of nucleosome mobilization by ISWI through PHD-histone contacts. EMBO J. 2004; 23:4029–4039. [PubMed: 15457208]
17. Clapier CR, Langst G, Corona DF, Becker PB, Nightingale KP. Critical role for the histone H4 N terminus in nucleosome remodeling by ISWI. Mol Cell Biol. 2001; 21:875–883. [PubMed: 11154274]
18. Hamiche A, Kang JG, Dennis C, Xiao H, Wu C. Histone tails modulate nucleosome mobility and regulate ATP-dependent nucleosome sliding by NURF. Proc Natl Acad Sci U S A. 2001; 98:14316–14321. [PubMed: 11724935]
19. Shogren-Knaak M, Ishii H, Sun JM, Pazin MJ, Davie JR, Peterson CL. Histone H4-K16 acetylation controls chromatin structure and protein interactions. Science. 2006; 311:844–847. [PubMed: 16469925]
20. Ferreira H, Flaus A, Owen-Hughes T. Histone modifications influence the action of Snf2 family remodelling enzymes by different mechanisms. J Mol Biol. 2007; 374:563–579. [PubMed: 17949749]
21. Valouev A, Johnson SM, Boyd SD, Smith CL, Fire AZ, Sidow A. Determinants of nucleosome organization in primary human cells. Nature. 2011; 474:516–520. [PubMed: 21602827]
22. Kagalwala MN, Glaus BJ, Dang W, Zofall M, Bartholomew B. Topography of the ISW2-nucleosome complex: insights into nucleosome spacing and chromatin remodeling. EMBO J. 2004; 23:2092–2104. [PubMed: 15131696]
23. Yamada K, et al. Structure and mechanism of the chromatin remodelling factor ISW1a. Nature. 2011; 472:448–453. [PubMed: 21525927]
24. Blosser TR, Yang JG, Stone MD, Narlikar GJ, Zhuang X. Dynamics of nucleosome remodelling by individual ACF complexes. Nature. 2009; 462:1022–1027. [PubMed: 20033040]
25. Ha T, Enderle T, Ogletree DF, Chemla DS, Selvin PR, Weiss S. Probing the interaction between two single molecules: Fluorescence resonance energy transfer between a single donor and a single acceptor. Proc Natl Acad Sci USA. 1996; 93:6264–6268. [PubMed: 8692803]
26. Deindl S, Hwang WL, Hota SK, Blosser TR, Prasad P, Bartholomew B, Zhuang X. ISWI Remodelers Slide Nucleosomes with Coordinated Multi-Base-Pair Entry Steps and Single-Base-Pair Exit Steps. Cell. 2013; 152:442–452. [PubMed: 23374341]
27. Mueller-Planitz F, Klinker H, Ludwigsen J, Becker PB. The ATPase domain of ISWI is an autonomous nucleosome remodeling machine. Nat Struct Mol Biol. 2013; 20:82–89. [PubMed: 23202585]
28. Fyodorov DV, Kadonaga JT. Binding of Acf1 to DNA involves a WAC motif and is important for ACF-mediated chromatin assembly. Mol Cell Biol. 2002; 22:6344–6353. [PubMed: 12192034]
29. Gelbart ME, Rechsteiner T, Richmond TJ, Tsukiyama T. Interactions of Isw2 chromatin remodeling complex with nucleosomal arrays: analyses using recombinant yeast histones and immobilized templates. Mol Cell Biol. 2001; 21:2098–2106. [PubMed: 11238944]
30. Narlikar GJ. A proposal for kinetic proof reading by ISWI family chromatin remodeling motors. Curr Opin Chem Biol. 2010; 14:660–665. [PubMed: 20833099]
31. Lowary PT, Widom J. New DNA sequence rules for high affinity binding to histone octamer and sequence-directed nucleosome positioning. J Mol Biol. 1998; 276:19–42. [PubMed: 9514715]
32. Luger K, Mader AW, Richmond RK, Sargent DF, Richmond TJ. Crystal structure of the nucleosome core particle at 2.8 A resolution. Nature. 1997; 389:251–260. [PubMed: 9305837]
33. Luger K, Rechsteiner TJ, Richmond TJ. Preparation of nucleosome core particle from recombinant histones. Methods Enzymol. 1999; 304:3–19. [PubMed: 10372352]
34. Rasnik I, McKinney SA, Ha T. Nonblinking and long-lasting single-molecule fluorescence imaging. Nat Methods. 2006; 3:891–893. [PubMed: 17013382]
35. Aitken CE, Marshall RA, Puglisi JD. An oxygen scavenging system for improvement of dye stability in single-molecule fluorescence experiments. Biophys J. 2008; 94:1826–1835. [PubMed: 17921203]

36. Kerssemakers JW, Munteanu EL, Laan L, Noetzel TL, Janson ME, Dogterom M. Assembly dynamics of microtubules at molecular resolution. Nature. 2006; 442:709–712. [PubMed: 16799566]

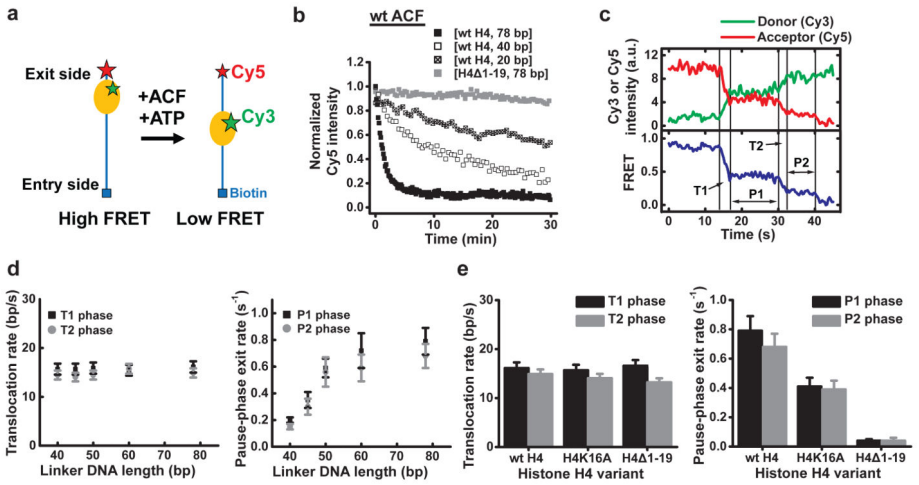

Figure 1. The linker DNA length and histone H4 tail regulate the remodelling pause phases but not the translocation phases

a, Schematic of a FRET-labelled mononucleosome undergoing remodelling by ACF. **b**, Ensemble remodelling time courses of [wt H4, 78 bp], [wt H4, 40 bp], [wt H4, 20 bp], and [H4Δ1-19, 78 bp] nucleosomes by 40 nM ACF at 5 μM ATP. Nucleosome translocation is monitored by the emission intensity of the FRET acceptor Cy5 under excitation of the FRET donor Cy3. **c**, Cy3 and Cy5 fluorescence (*top*) and FRET (*bottom*) time traces during the remodelling of a single [wt H4, 78 bp] nucleosome with the translocation (T1, T2) and pause (P1, P2) phases indicated. **d**, Linker DNA length dependence of the translocation rates between pauses (*left*, defined as the average number of base pairs moved per second) and pause-phase exit rates (*right*, defined as the inverse of the average pause durations). **e**, Dependence of the translocation rates between pauses (*left*) and pause-phase exit rates (*right*) on the H4 variants. In (d) and (e), [ACF] = 10 nM and [ATP] = 2 mM. Data are mean ± s.e.m. derived from at least 100 (d) or at least 50 (e) individual nucleosome remodelling traces from three independent experiments.

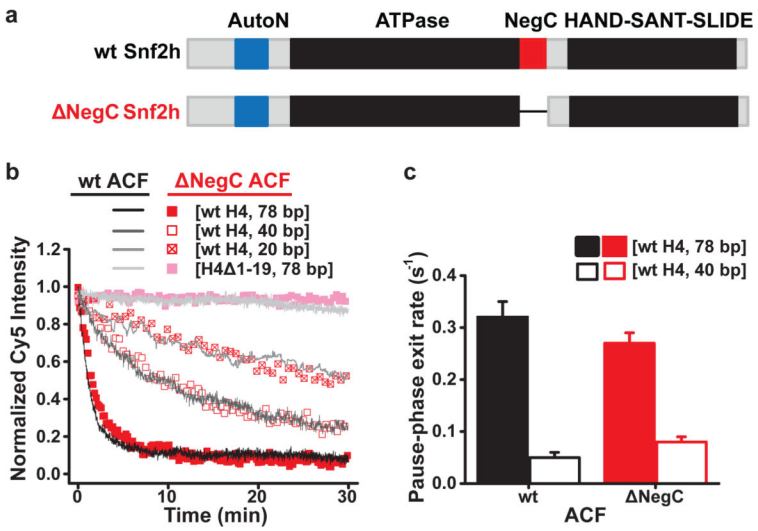

Figure 2. Deletion of the NegC domain of the Snf2h catalytic subunit does not substantially affect linker DNA length sensing by the ACF complex

a, Domain architecture of wt and ΔNegC Snf2h (residues 669-700 replaced with a SGSGS linker). **b**, Ensemble remodelling time courses of [wt H4, 78 bp], [wt H4, 40 bp], [wt H4, 20 bp], and [H4Δ1-19, 78 bp] nucleosomes by 40 nM wt ACF (black/gray lines, duplicated from Fig. 1b) and ΔNegC ACF (red/pink symbols) at 5 μM ATP. **c**, Linker DNA length dependence of the pause-phase exit rate (P1 phase) measured for wt ACF (black) and ΔNegC ACF (red). [ACF] = 10 nM and [ATP] = 20 μM. Data are mean ± s.e.m. derived from at least 100 individual nucleosome remodelling traces from three independent experiments.

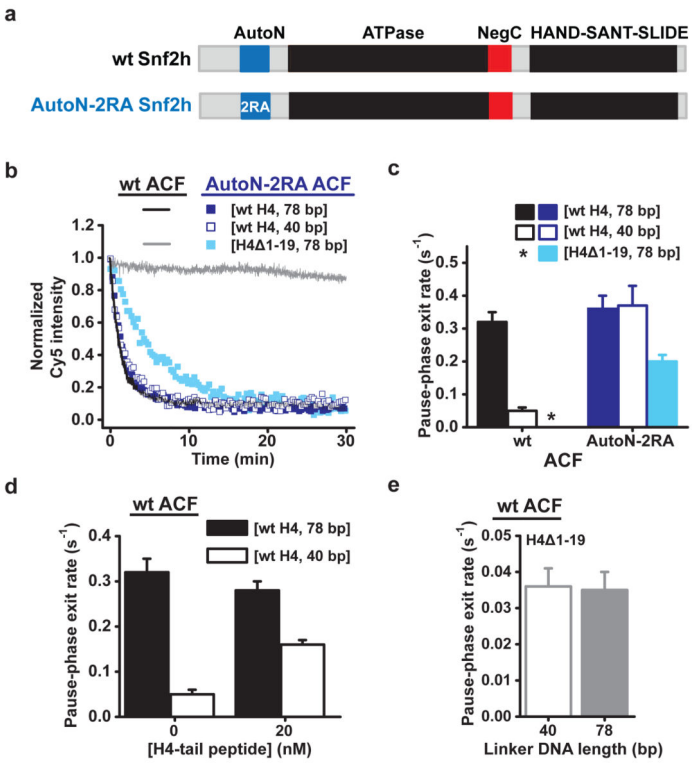

Figure 3. The AutoN domain of Snf2h and the nucleosomal H4 tail are important for linker DNA length sensing by the ACF complex

a, Domain architecture of wt and AutoN-2RA (R142A and R144A) Snf2h. **b**, Ensemble remodelling time courses of [wt H4, 78 bp], [wt H4, 40 bp] and [H4Δ1-19, 78 bp] nucleosomes by 40 nM wt ACF (black/gray lines, duplicated from Fig. 1b) and AutoN-2RA ACF (blue/cyan symbols) at 5 μM ATP. **c**, Dependence of the pause-phase exit rate on the linker DNA length and H4 tail for wt (black) or AutoN-2RA ACF (blue/cyan). * too slow to be measured. **d**, Effect of the exogenously added H4-tail peptide on the pause-phase exit rates during remodelling by wt ACF. **e**, Pause-phase exit rates of nucleosomes lacking the H4 tail during remodelling by wt ACF. In (c-f), [ACF] = 10 nM and [ATP] =20 μM, except that 2 mM of ATP was used in (e) to make the pause exit rates measurable for nucleosomes lacking the H4 tail. Data are mean ± s.e.m from at least 100 (c, d) or at least 50 (e) individual nucleosome remodelling traces from three independent experiments.

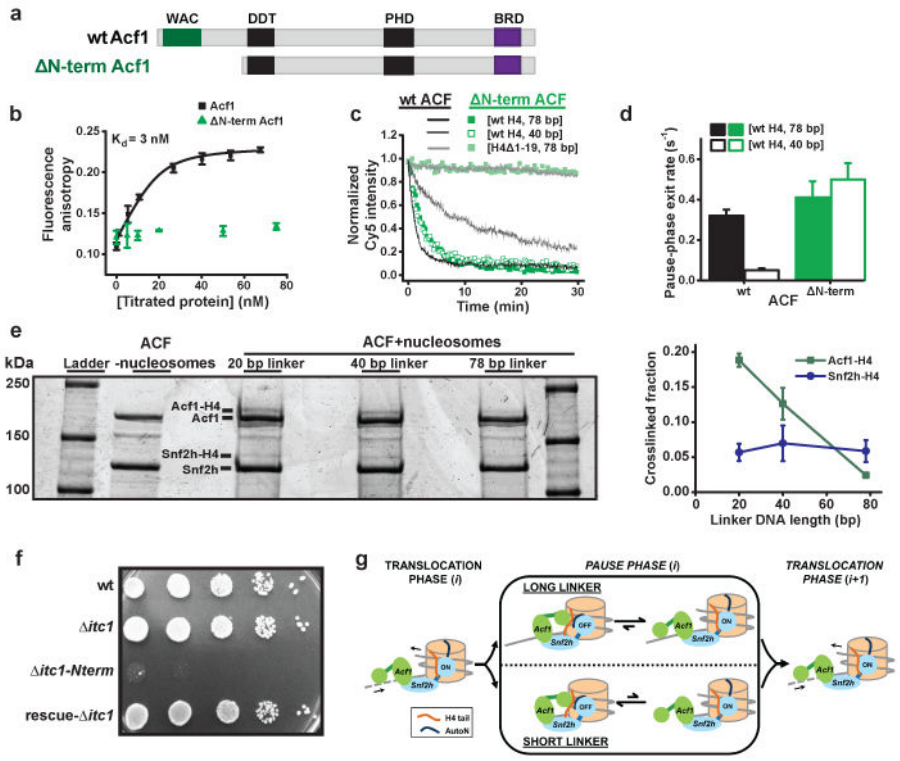

Figure 4. The N-terminal region of the Acf1 accessory subunit is important for linker DNA length sensing by the ACF complex

a, Domain architecture of wt and ΔN-term (residues 1-371 deleted) Acf1. **b**, Fluorescence anisotropy of dye-labelled H4-tail peptide in the presence of varying amounts of wt (black symbols) or ΔN-term (green symbols) Acf1. Data are mean ± s.e.m. (*n*= 3 independent experiments). The K_d for wt Acf1 is 3 ± 9 nM (error represents the 95% confidence interval). **c**, Ensemble remodelling time courses of [wt H4, 78 bp], [wt H4, 40 bp], and [H4Δ1-19, 78 bp] nucleosomes by 40 nM wt ACF (black/gray lines, duplicated from Fig. 1b) and ΔN-term ACF (green/light green symbols) at 5 μM ATP. **d**, Dependence of the pause-phase exit rate on the linker DNA length for wt ACF (black) or ΔN-term ACF (green). [ACF] = 10 nM and [ATP] = 20 μM. Data are mean ± s.e.m derived from at least 100 individual nucleosome remodelling traces from three independent experiments. **e**, Crosslinking of the H4 tail to Acf1 depends on the linker DNA length. The crosslinking products were analysed by SDS-PAGE (*left*). The Acf1-H4 crosslinking band was absent for ACF without nucleosomes (lane "- nucleosomes"). (*right*) Quantification of the H4-crosslinked fractions of Acf1 and Snf2h as a function of linker DNA length. Data are mean ± s.e.m. (*n*= 3 independent crosslinking experiments). **f**, Effects of deletion of Itc1 (Acf1 homolog) and its N-terminal region on the growth of yeast cells. Top row: wt. Second row: the *itc1* gene is deleted (Δ*itc1*). Third row: the coding sequence of the N-terminal region of Itc1 is deleted (Δ*itc1-Nterm*). Bottom row: The remaining portion of *itc1* is deleted from Δ*itc1-Nterm* (rescue-Δ*itc1*). One representative of three independent growth experiments is shown. **g**, Model for linker DNA length sensing by the ACF complex. DNA: gray lines, histone octamer: beige cylinders, Snf2h: blue/cyan, Acf1: green. The ATPase domain of

Snf2h is depicted as a cyan sphere and labelled “ON” when active and “OFF” when inactive.